J. Fluid Mech. (2009), *vol.* 633, *pp.* 411–423.
doi:10.1017/S0022112009007964 Printed in the United Kingdom

Vortex wakes of a flapping foil

TEIS SCHNIPPER, ANDERS ANDERSEN† AND TOMAS BOHR

Department of Physics and Center for Fluid Dynamics,
Technical University of Denmark, DK-2800 Kgs. Lyngby, Denmark

(Received 4 February 2009 and in revised form 29 April 2009)

We present an experimental study of a symmetric foil performing pitching oscillations in a vertically flowing soap film. By varying the frequency and amplitude of the oscillation we visualize a variety of wakes with up to 16 vortices per oscillation period, including von Kármán vortex street, inverted von Kármán vortex street, 2P wake, 2P+2S wake and novel wakes ranging from 4P to 8P. We map out the wake types in a phase diagram spanned by the width-based Strouhal number and the dimensionless amplitude. We follow the time evolution of the vortex formation near the round leading edge and the shedding process at the sharp trailing edge in detail. This allows us to identify the origins of the vortices in the 2P wake, to understand that two distinct 2P regions are present in the phase diagram due to the timing of the vortex shedding at the leading edge and the trailing edge and to propose a simple model for the vorticity generation. We use the model to describe the transition from 2P wake to 2S wake with increasing oscillation frequency and the transition from the von Kármán wake, typically associated with drag, to the inverted von Kármán wake, typically associated with thrust generation.

1. Introduction

Vortex formation and organization are key components in fluid-structure interaction at intermediate and high Reynolds numbers, and insight into vortex processes is central for understanding many phenomena ranging from how a swimming fish generates propulsive forces to how an offshore structure is influenced by the flow around it. The periodic shedding of vortices leading to the von Kármán vortex street behind a cylinder in a free stream provides the classical example of vortex formation behind a stationary object. A great variety of wakes can be formed by oscillating the cylinder laterally in the free stream as shown in the seminal work by Williamson & Roshko (1988). The wakes behind the oscillating cylinder include von Kármán-type wakes in which two vortices of opposite sign are shed per oscillation period (2S) and wakes in which two vortex pairs are shed per oscillation period (2P). These wake types occur more generally behind oscillating structures such as aerofoils. Bratt (1953) visualized 2S wakes and Koochesfahani (1986, 1989) visualized 2S and 2P wakes behind an aerofoil performing pitching oscillations in a free stream. Similarly Lai & Platzer (1999) observed 2S and 2P wakes behind an aerofoil with plunging oscillations, and Buchholz & Smits (2008) visualized the three-dimensional wake structures behind a pitching foil with low aspect ratio. Recently Godoy-Diana, Aider

† Email address for correspondence: aanders@fysik.dtu.dk

& Wesfreid (2008) measured the von Kármán wakes and the inverted von Kármán wakes behind a flapping hydrofoil using particle image velocimetry. The transition from the von Kármán wake to the inverted von Kármán wake occurs as the vortices cross the centreline, and it is linked with the transition from drag to thrust production (von Kármán & Burgers 1935). The inverted von Kármán wake therefore plays an important role in biological locomotion (Lighthill 1969; Sfakiotakis, Lane & Davies 1999; Triantafyllou, Triantafyllou & Yue 2000); also, more complex wakes such as 2P are of importance for fish swimming (Müller *et al.* 2001; Müller, van den Boogaart & van Leeuwen 2008).

In the present experiment we investigate the wakes formed by a rigid foil in a two-dimensional free stream created by a vertically flowing soap film. The symmetric foil has a round leading edge and a sharp trailing edge, and it is driven with simple harmonic pitching oscillations. The experiment is characterized by three dimensionless parameters that we can vary independently, i.e. the width-based Strouhal number

$$St_D = \frac{D\,f}{U}, \tag{1.1}$$

the dimensionless amplitude

$$A_D = \frac{2\,A}{D} \tag{1.2}$$

and the Reynolds number

$$Re = \frac{D\,U}{\nu}, \tag{1.3}$$

where D is the width of the foil; f is the frequency of the simple harmonic oscillation; U is the free-stream flow speed; A is the flapping amplitude; and ν is the kinematic viscosity of the flowing soap film. Although a flowing soap film is more complex than an incompressible Newtonian flow (Couder, Chomaz & Rabaud 1989; Chomaz & Cathalau 1990), the types of wakes appear to be the same. The great advantage of the soap film is the ease and precision with which the flow can be visualized, and in addition to the wake structures, we have thus been able to visualize the evolution of the boundary layers on the sides of the foil and the vortex-shedding process in remarkable detail.

The soap film tunnel is an efficient tool for mapping out the possible wakes behind the foil and exploring their dependence on the frequency and amplitude of the pitching oscillations. The idea of obtaining an overview of measured wakes at constant Reynolds number using a map (phase diagram) in the frequency and amplitude plane goes back to Williamson & Roshko (1988) who made a detailed map for the cylinder oscillating laterally in a free stream. The phase diagram was later considered by Ponta & Aref (2005) who developed a simple model that explains measured locations of important wake transitions. Godoy-Diana *et al.* (2008) recently measured a phase diagram for the wakes of a pitching foil with focus on 2S wakes and drag–thrust transition. We construct our wake map by scanning the amplitude continuously at constant frequency, and in addition to the 2S wakes observed by Godoy-Diana *et al.* (2008) we find a wide selection of wakes, including 2P wakes which were visualized by Koochesfahani (1986, 1989), 2P+2S wakes which are known for oscillating cylinders (Williamson & Roshko 1988) and a series of novel wakes with up to 16 vortices per oscillation period at low oscillation frequencies. We show that the idea by Ponta & Aref (2005) can be adapted to explain the oscillation

frequency dependence of the number of vortices formed per oscillation period for these wakes.

The measured phase diagram allows us to investigate two of the significant wake transitions, namely the 2P to 2S transition with increasing oscillation frequency and the transition from the von Kármán wake to the inverted von Kármán wake. The round leading edge and the sharp trailing edge of the oscillating foil give rise to two distinct sources of vorticity, i.e. the boundary layers along the two sides of the foil and the trailing edge which experiences the pitching oscillations of the foil. The vorticity production at the trailing edge depends on the frequency and amplitude of the pitching oscillations. Applying ideas that go back to Prandtl & Tietjens (1934) we give a simple estimate of the vorticity production and show how to apply it to describe the nature of the 2P to 2S transition and the transition from the von Kármán wake to the inverted von Kármán wake.

The soap film tunnel is also advantageous, since it makes it possible to follow the wake downstream for up to 20 oscillation periods and to visualize the far-wake evolution. Thereby our experiment allows us to explore wake instabilities, and it provides a test ground for point vortex models of exotic wakes (Aref, Stremler & Ponta 2006). This aspect of the experiment is not the main focus of the present paper, and we shall only describe a few characteristic features of the far-wake evolution.

2. Experimental set-up

Our set-up makes use of a gravity-driven, vertically flowing soap film which functions as a two-dimensional flow tunnel as reviewed by Rutgers, Wu & Daniel (2001). Since the pioneering works of Couder & Basdevant (1986) and Gharib & Derango (1989), flowing soap films have been used to study many different phenomena, including two-dimensional turbulence (Rivera, Vorobieff & Ecke 1998), cylinder wakes (Vorobieff & Ecke 1999), vortices shed by a flexible filament (Zhang *et al.* 2000) and wakes of a heaving and pitching foil (Lentink *et al.* 2008). In our set-up soapy water consisting of 1.5 % dish washing soap (Fairy Ultra) in demineralized water flows from the upper reservoir between two nylon wires (0.1 cm in diameter) and produces a planar soap film (15.2 cm in width) as sketched in figure 1(*a*). Due to air drag a terminal velocity is reached, and the soap film has uniform free-stream velocity profile and constant thickness in the test section. An overflow mechanism in the upper reservoir ensures a constant pressure head at the flow regulation valve and allows the average flow speed U in the test section to be held constant to within 5 %. In our experiment we typically have $U = 150$ cm s^{-1} and a film thickness of 1.5 μm. We measure the velocity by tracking small air bubbles in the flowing film. It is difficult to accurately determine the kinematic viscosity of the soap film. Inspired by Vorobieff & Ecke (1999) we measure the shedding frequency of vortices behind stationary cylinders (with diameters from 0.1 mm to 12 mm) and use the Reynolds-number-versus-Strouhal-number curve to obtain the estimate $\nu = 0.07$ cm^2 s^{-1}, which is approximately seven times the kinematic viscosity of pure water.

The soap film is penetrated perpendicularly in the test section by a rigid foil as sketched in figure 1(*b*). The foil is milled out of brass and has a semicircular leading edge with diameter D, chord length C and straight sides that form a sharp trailing edge. We presume that the wake structures will be qualitatively similar for foils with different chord-to-width ratio provided that C/D is larger than approximately two, so that the round leading edge and the sharp trailing edge are clearly separated. We use a foil with $D = 0.10$ cm and $C = 0.60$ cm for our measurements with $St_D < 0.15$,

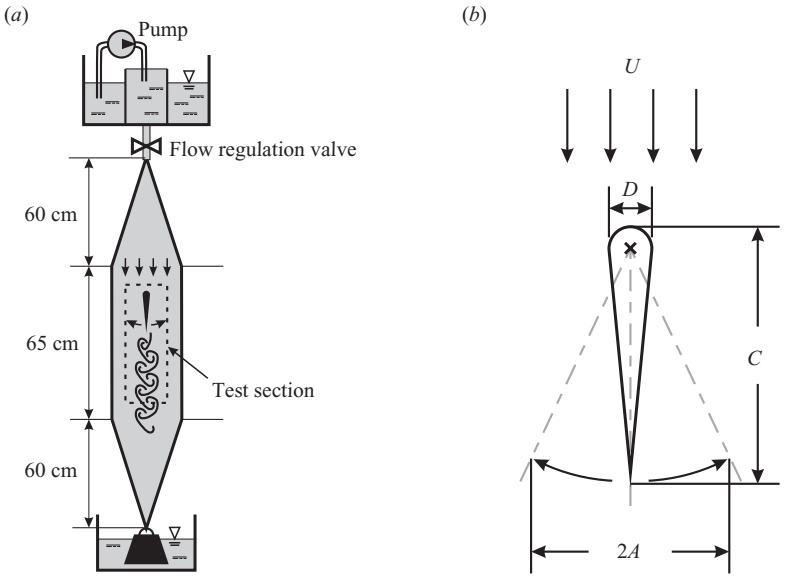

FIGURE 1. Schematic illustrations of (*a*) the soap film tunnel and (*b*) the oscillating foil.

and for our measurements with $St_D > 0.15$ we use a foil with $D = 0.20$ cm and $C = 1.20$ cm. With the values given above for U and ν we have $Re = 220$ for the small foil and $Re = 440$ for the large foil. To test if the choice of foil had any influence on the observed transitions we made selected scans with the small foil at $St_D > 0.15$ and with the large foil at $St_D < 0.15$. With the two foils we found the same wake structures and transitions. We presume that the qualitative structure of the phase diagram is insensitive to the value of the Reynolds number in the intermediate range between 10^2 and 10^4, since our two-dimensional flow is not subject to three-dimensional instabilities. The foil is mounted on a shaft and is oscillated with simple harmonic pitching oscillations. A spring mechanism is connected to the shaft such that it experiences a restoring torque when rotated away from the zero-angle orientation by a motor, which is controlled by a sine-wave generator with adjustable amplitude and frequency (30–230 Hz). We monitor the foil oscillation by reflecting a laser beam off a mirror mounted on the shaft and following its motion on a projection screen with high-speed digital video. The resulting motion of the foil is sinusoidal everywhere in the phase diagram.

The soap film behaves as a two-dimensional incompressible fluid when the flow speeds are low compared to the speed of the elastic (longitudinal Marangoni) waves in the soap film (Couder *et al.* 1989; Chomaz & Cathalau 1990). In our soap film we estimate that the Marangoni wave speed is approximately 10^3 cm s^{-1} (Couder *et al.* 1989). The largest flow speeds in the soap film are set by the maximum speed of the foil tip, which in the parameter region that we consider is approximately 3×10^2 cm s^{-1}. The Marangoni wave speed is therefore considerably larger than the flow speeds, and we do not expect any significant effects of compressibility. The qualitative structure of the flow in the soap film can be visualized by following thickness variations which are created as the vortices form and are advected along with the flow as a passive scalar (Rivera *et al.* 1998). We visualize the thickness variations in the standard way by using a monochromatic light source (low-pressure sodium lamp, Philips SOX90) which gives rise to interference fringes formed by the light reflected at the front and

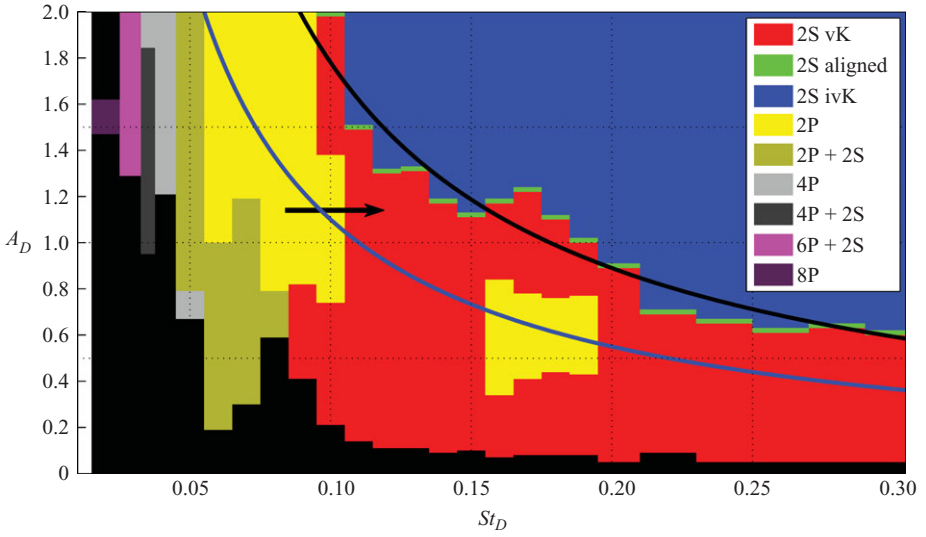

FIGURE 2. Phase diagram of vortex synchronization regions spanned by the width-based Strouhal number and the dimensionless amplitude. The colour shows the type of wake observed. A narrow 6P region (not indicated) exists between the 4P+2S and 6P+2S areas. Along each solid line the amplitude-based Strouhal number is constant with the values $St_A = 0.11$ (blue) and $St_A = 0.18$ (black). The arrow indicates the 2P to 2S transition discussed in § 5. In the black regions at low frequency and amplitude we did not observe a synchronized wake. At $St_D < 0.15$ we used the small foil ($D = 0.10$ cm), and at $St_D > 0.15$ we used the large foil ($D = 0.20$ cm). In the legend, 'vK' is for von Kármán and 'ivK' is for inverted von Kármán.

at the back of the film. The difference in thickness between interference fringes is 0.22 μm. We record the time evolution of the interference patterns using a digital high-speed camera (Phantom v4.2 monochrome) at typically 4000 frames s^{-1}. To obtain still pictures with high resolution we use a digital camera (Nikon D70s) with a macro-objective (Nikon AF-S VR Micro-Nikkor 105 mm f/2.8G IF-ED).

3. Phase diagram

We measured the phase diagram in the (St_D, A_D) plane in the following way. We first adjusted the frequency to a selected value and then slowly varied the amplitude continuously to scan for changes in wake structure. We identified the wake transitions visually in high-speed digital video sequences by scanning with both increasing and decreasing amplitude and without observing any hysteresis. In all cases the high-speed video recordings of the flow allowed us to identify the centre and the sense of rotation of each vortex. We observed the flow for several consecutive periods of oscillation to determine whether or not the pattern was synchronized with the periodic oscillation of the foil. Figure 2 shows the phase diagram in the region $0 < St_D < 0.3$ and $0 < A_D < 2$ with the resolution in St_D indicated by the column width. The wake regions are labelled using the symbols introduced by Williamson & Roshko (1988), where 'S' signifies a single vortex and 'P' signifies a pair of vortices of opposite signs.

The region with $0.1 < St_D < 0.3$ is dominated by 2S wakes, i.e. von Kármán vortex street at small A_D and inverted von Kármán vortex street at large A_D. Figure 3 shows typical examples of (*a*) the von Kármán wake and (*b*) the inverted von Kármán wake. As the von Kármán wake is advected downstream, the vortices leave the

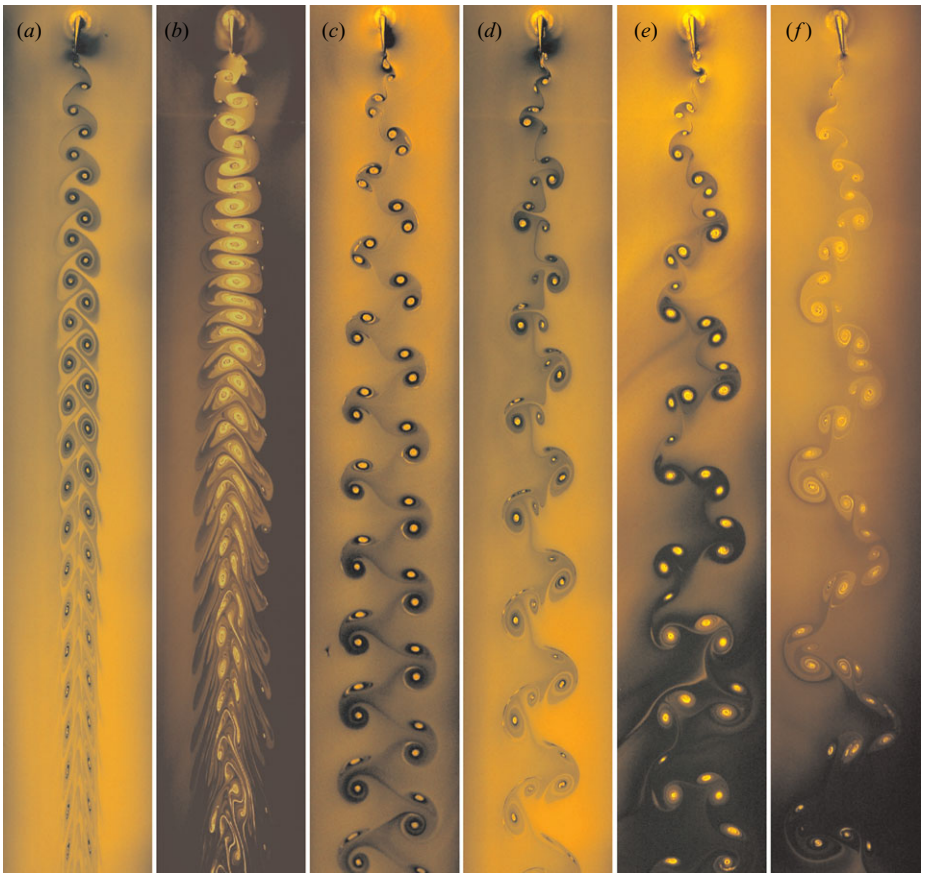

FIGURE 3. Selected wakes with the small foil: (*a*) von Kármán wake for $St_D = 0.12$ and $A_D = 0.98$; (*b*) inverted von Kármán wake for $St_D = 0.12$ and $A_D = 2.0$; (*c*) 2P wake for $St_D = 0.080$ and $A_D = 1.4$; (*d*) 2P+2S wake for $St_D = 0.053$ and $A_D = 1.2$; (*e*) 4P wake for $St_D = 0.039$ and $A_D = 1.34$; and (*f*) 4P+2S wake for $St_D = 0.035$ and $A_D = 1.47$.

classical staggered arrangement to form a double-row configuration. In contrast, the stronger and closer-lying vortices in the inverted von Kármán wake induce large strain rates, which tear the individual vortices apart and leave a blurred wake without clear vortex structures. The transition between the two wake types occurs with the vortices aligned on the centreline. The solid black line in figure 2 is a line with constant amplitude-based Strouhal number $St_A = 2Af/U$. More specifically we see in agreement with Godoy-Diana *et al.* (2008) that the boundary between the von Kármán wake and the inverted von Kármán wake is approximately at $St_A = 0.18$. We note that a region with 2P wakes exists as a small island in the phase diagram surrounded by 2S wakes. We return to this in the following section and explain the mechanism behind the formation of 2P wakes. When the foil is not oscillated a 2S wake appears, but the vortices do not form immediately behind the trailing edge in contrast to the oscillating case. Instead they only become clearly visible approximately two chord lengths downstream of the trailing edge due to a wake instability. We note that we exclusively find wakes with left–right symmetry and that we do not scan the parameter region in which wakes with broken left–right symmetry are present (Godoy-Diana *et al.* 2008, 2009). Further, in the entire phase diagram (with the

exception of the black regions) the frequency of the wake pattern is locked with the frequency of the external oscillation of the foil.

The part of the phase diagram with $0 < St_D < 0.1$ contains wakes in which more than two vortices are shed per oscillation period, since the frequency is low in comparison with the frequency for vortex separation in the side boundary layers. Figure 3(*c–f*) respectively shows examples of a 2P wake, a 2P+2S wake, a 4P wake and a 4P+2S wake. The 2P wakes are found in two large parameter regions, and they resemble the 2P wake visualized by Koochesfahani (1986, 1989) behind an NACA 0012 aerofoil with pitching oscillations. Figure 3(*c*) shows the evolution of the 2P wake downstream for 10 oscillation periods. We clearly see how the vortex pairs move away from the centreline and slowly turn anticlockwise (clockwise) on the left-hand (right-hand) side of the centreline, indicating that the downstream vortex is slightly stronger than the upstream vortex in each pair. By decreasing St_D or A_D we move from 2P wakes to the complex 2P+2S wakes (figure 3*d*) with single vortices between vortex pairs, and with a further decrease of St_D we observe 4P wakes (figure 3*e*), 4P+2S wakes (figure 3*f*) and so on up to 8P wakes. We have seen 6P wakes between the 4P+2S and 6P+2S areas, but sensitivity of the system at these low St_D prevents clear identification of a 6P region, and it is therefore not shown in the phase diagram. The overall wavy appearance of the 4P+2S wake in figure 3(*f*) reflects the trajectory of the sharp trailing edge relative to the free-stream flow. The 4P+2S, 6P, 6P+2S and 8P wakes all share this feature which is characteristic of the wakes at low St_D and high A_D. In general the total number of vortices in each period is even due to the left–right symmetry of the system, and the total number of vortices increases as St_D is lowered and the oscillation period increased. To describe this trend at low St_D we suggest a simple idea which is inspired by the model by Ponta & Aref (2005) for the number of vortices formed per period in the experiment by Williamson & Roshko (1988). We assume that the Strouhal number for vortex separation in the side boundary layers is identical to the Strouhal number for flow past a fixed cylinder $St_0 = D\,f_0/U$, where f_0 is the shedding frequency. With the same experimental conditions as for the foil we have measured $St_0 = 0.17$ for a cylinder with diameter $D = 0.10$ cm. For the slowly flapping foil we presume that the circulation production at the sharp trailing edge is insignificant in comparison with the circulation production in the side boundary layers. We therefore estimate that the vortex-shedding frequency is given approximately by f_0, with the constraint that the entire vortex pattern is, at sufficiently large amplitude, locked to the driving frequency f. With our assumptions, the total number of vortices that form in one oscillation period is the integer nearest to $m = 2\,St_0/St_D$. The simple model, e.g., predicts $m = 6$ at $St_D = 0.057$ and $m = 16$ at $St_D = 0.021$ in agreement with the location of the 2P+2S region and the 8P region in the phase diagram. The model predicts that the boundaries between different wake regions are lines of constant St_D. This is evidently not the case for all boundaries in the phase diagram, including the boundary between 2P and 2P+2S in the range $0.055 < St_D < 0.085$. However, in the regions with many vortices per period in which the model assumptions hold, the boundaries are indeed lines of constant St_D in agreement with the model prediction.

4. Formation of 2P wake

Figure 4 shows five snapshots during half of the flapping cycle as the foil moves from the leftmost position to the rightmost position. In frame (*a*), two vortices are close to the trailing edge: one with positive (anticlockwise) circulation (A), located

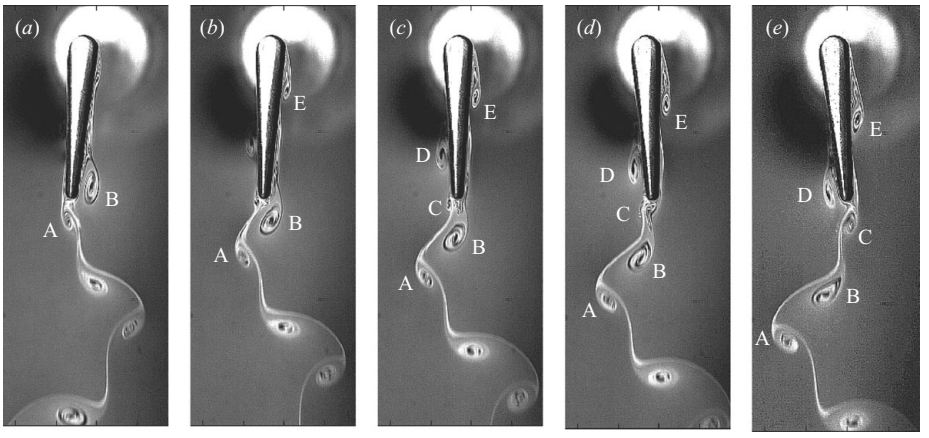

FIGURE 4. Time-series of the vortex formation during half a flapping cycle creating a 2P wake with $St_D = 0.09$ and $A_D = 0.95$ behind the small foil. Time advances to the right.

immediately under the foil tip, and one with negative circulation (B) on the right side of the foil. In frame (*b*), A is shed into the wake, while B is just about to be shed. Meanwhile, the vortical structures D and E in the boundary layers are rolling down the side of the foil. The centres of D and E move with approximately half of the free-stream flow speed. A simple picture of the vortex motion is therefore that of a rigid wheel rolling on a surface without slipping. The tip speed is at its maximum as the foil passes the centreline in frame (*c*), and consequently the vorticity production due to the tip movement is large. This leads to the creation of the vortex C in frames (*d*) and (*e*). In frame (*e*), the foil is in the rightmost position, and the vortex C is shed. Following this frame, D is shed and travels with C as a pair. In frames (*b*)–(*e*), A and B are advected downstream as a pair while translating away from the centreline due to their mutual advection. In summary we therefore see that a vortex pair in the wake on one side of the centreline consists of vortices that were initially formed on the opposite side of the centreline and that the downstream vortex in the pair was formed due to the tip movement while the upstream vortex in the pair was formed in the boundary layer. In addition we clearly see the frequency locking to the external drive. The situation in (*e*) is equivalent to that in (*a*) with C replacing A and D replacing B; so the same sequence of events will take place in the next half-stroke (when the foil moves from right to left) except that all vorticity will be reversed.

The 2P formation scenario, in which each left (right) leading edge vortex forms when the foil is at the rightmost (leftmost) position, advects along the side of the foil with approximately half of the free-stream flow speed and forms a vortex pair together with the tip vortex formed in the previous half-period, is possible if the time that it takes for the leading edge vortex to advect one chord length is approximately equal to an integer number of oscillation periods. It turns out that the 2P formation follows this scenario also in the 2P region in the range $0.155 < St_D < 0.195$ as we explain in the following. The time T for the vortex to travel one chord length is $T = 2C/U$, since $U/2$ is the advection speed. The advection time is therefore $T = 12\,St_D/f$, and the time is equal to one oscillation period at $St_D = 1/12 \approx 0.083$ and equal to two oscillation periods at $St_D = 1/6 \approx 0.17$. These parameter values fall within the two 2P regions in the phase diagram, and our high-speed digital video recordings of the 2P formation in the small region do indeed show two vortices which travel downstream on each side of the foil separated by half a chord length. In the

region with $St_D > 0.1$ we find that two vortices form in the boundary layers on the sides of the foil and two vortices form at the tip in each oscillation period. Our simple model does not provide a prediction for the extension of the 2P regions. To obtain such a prediction we would need to be able to predict the strengths and sizes of the vortices and determine a precise criterion on the vortex separation distance for when coalescence of the same-sign vortex structures formed in a given period will take place. Special conditions like the 2P scenario described above are required for the four vortex patches not to coalesce two-by-two and lead to a 2S wake. The formation of complex wake patterns with more than two vortices per oscillation period at high oscillation frequencies therefore turns out to be possible only on the small 2P island in the 2S ocean.

It is interesting to note that despite the differences in geometry and kinematics, the boundary between the 2S region and the main 2P region in our experiment is qualitatively similar to the boundary between 2S and 2P found by Williamson & Roshko (1988) for a cylinder oscillating laterally in a free stream. However, there are also qualitative differences between the two phase diagrams, e.g. the existence of the single 2P region for the cylinder in contrast to the two distinct 2P regions for the foil. The scenarios for 2P formation are also qualitatively different for the two systems. The vortex pairs in the 2P region behind the cylinder consist of vortices initially formed in the boundary layers on the cylinder. Williamson & Roshko (1988) described that four vortex patches are formed per period, one in each boundary layer per half-period of the prescribed motion. Each vortex pair therefore consists of a vortex formed to the left and a vortex formed to the right of the trajectory of the cylinder centre. In contrast, both vortices in a pair on a given side of the centreline in our experiment are initially formed on the opposite side of the foil, one at the leading edge and one at the trailing edge.

Wakes in which two vortex pairs are shed per oscillation period, i.e. 2P wakes, play a role in fish swimming and have been observed using particle image velocimetry behind freely swimming eel (Müller *et al.* 2001) and zebra fish larva (Müller *et al.* 2008). These measurements revealed that vorticity is created along the body and at the tail, but the complexity of the measured velocity fields prevented a clear identification of the vortex origins (Müller *et al.* 2001, 2008). Our 2P wakes are most likely drag wakes, since the vortex pairs point upstream and away from the centreline as shown in figure 3(*c*). In contrast, the vortex pairs behind the swimming fish point downstream and away from the centreline, which indicates that the fish produces thrust and large lateral forces (Müller *et al.* 2008). Despite these differences and the obvious three-dimensionality of the fish, we believe that the 2P wakes behind fish could form following the 2P formation scenario described above.

5. Wake transitions

The wake transition from 2P to 2S with increasing oscillation frequency involves a change in the timing of the vortex shedding and in the strength of the vorticity production at the tip and in the side boundary layers. Figure 5 shows wakes on the transition path indicated by the arrow in figure 2. Each picture is taken when the foil is in the rightmost position. The vortex pairs in frame (*a*) consist of vortices of comparable strength, which form as discussed previously. In frame (*b*) the same-sign vortices have moved closer together, and the distance between the two vortices in each pair has increased. In frame (*c*) this effect is more apparent and the upstream (boundary layer) vortex in each pair is weaker than the downstream (trailing edge)

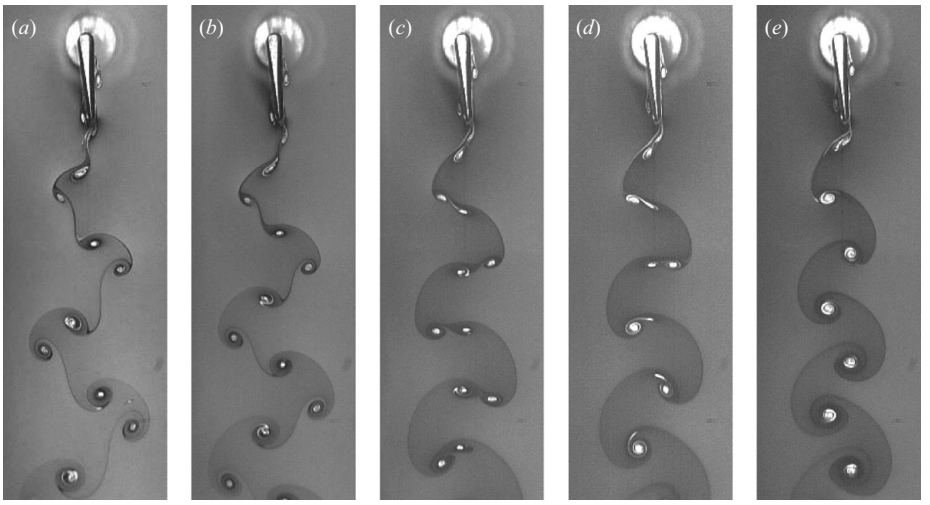

FIGURE 5. Snapshots of the wake at the rightmost position of the small foil when following the transition path from 2P to 2S indicated by the arrow in the phase diagram. The dimensionless amplitude was held constant at $A_D = 1.14$, while the width-based Strouhal number was varied: (*a*) $St_D = 0.084$, (*b*) $St_D = 0.096$, (*c*) $St_D = 0.105$, (*d*) $St_D = 0.109$ and (*e*) $St_D = 0.12$.

vortex. In frame (*d*) the strong downstream vortex in a pair merges with the same-sign upstream vortex in the pair formed immediately before to form a single vortex. In frame (*e*) the two vortices merge during the shedding at the tip, and the wake appears to be a von Kármán-type 2S wake.

To understand the relative strengths of the two vortices appearing in the pairs of the 2P wakes we will now introduce simple estimates of their circulations. The magnitude of the circulation Γ_{BL} formed in the boundary layer on one side of the foil during one half-period can be estimated by considering the downward transport of vorticity in the boundary layer with no-slip on the foil and free-stream flow speed U. Using the estimate for vorticity production in Prandtl & Tietjens (1934) we find

$$\Gamma_{BL} = \frac{1}{2}\int_0^{1/2f} U^2 \,\mathrm{d}t = \frac{U^2}{4f} = \frac{D\,U}{4\,St_D}. \tag{5.1}$$

It is more difficult to estimate the circulation Γ_{TE} formed at the tip due to the flapping motion with the foil moving either left or right. As a simplistic estimate we neglect the free-stream flow and take only the motion of the trailing edge into account,

$$\Gamma_{TE} = \frac{1}{2}\int_0^{1/2f} V_{TE}^2(t)\,\mathrm{d}t \approx \frac{1}{2}\pi^2 A^2 f = \frac{1}{8}\pi^2 A_D^2\, St_D\; D\,U, \tag{5.2}$$

where V_{TE} is the magnitude of the velocity of the trailing edge and where the approximate equality is valid at the low oscillation amplitudes of our experiment. We presume that (5.1) is a fair estimate of the circulation formed in each boundary layer, whereas (5.2) underestimates the actual vorticity production at the tip and is only valid when the flapping motion is totally dominant. Nevertheless, the ratio of the two circulation estimates $\Gamma_{TE}/\Gamma_{BL} \approx \pi^2\, St_A^2/2$ suggests the significance of the amplitude-based Strouhal number in determining the increase of the strength of the trailing edge vortex relative to the strength of the leading edge vortex in qualitative agreement with the visualizations in figure 5. We also note that we see approximately

the same value of St_A in the two 2P regions as indicated by the solid blue line in figure 2.

The amplitude-based Strouhal number is of great importance for the transition between the von Kármán wake and the inverted von Kármán wake, which takes place approximately at $St_A = 0.18$ as shown in figure 2. Indeed the circulation estimates (5.1) and (5.2) suggest that the transition between the von Kármán wake and the inverted von Kármán wake should occur when the strength of the trailing edge vortices exceeds the strength of the boundary layer vortices. The location of the wake transition was observed experimentally by Godoy-Diana *et al.* (2008), who also determined the drag–thrust transition and found that it takes place at a slightly larger amplitude-based Strouhal number and thus does not exactly coincide with the transition to the inverted von Kármán wake. Similar experimental results have recently been obtained using molecular tagging velocimetry by Bohl & Koochesfahani (2009). It is well established experimentally that propulsive efficiency peaks in an amplitude-based Strouhal number interval close above the transition (Anderson *et al.* 1998), but theory for the drag–thrust transition is limited to ideal fluid models. Garrick (1936, pp. 1–9) determined the drag–thrust transition theoretically for a plate with simple harmonic pitching oscillations of small amplitude in an ideal fluid. The transition from drag to thrust is in that case independent of the oscillation amplitude, and with pitching oscillations about the 1/4 chord point the transition takes place at $St_D = 1/(6\pi) \approx 0.05$. In a real fluid the drag–thrust transition takes place at larger values of St_D, and its dependence on A_D does not follow from the ideal fluid model as pointed out by Koochesfahani (1989).

6. Conclusions

We have presented the phase diagram for a flapping foil in a flowing soap film in the vicinity of the drag–thrust transition. Our phase diagram has revealed a rich variety of vortex wakes ranging from 2S and 2P to complex wakes with up to 16 vortices per oscillation period that to our knowledge have not been observed before. Our flow visualizations allow us to pinpoint the essential features of the vortex formation process and to describe a number of characteristics of the phase diagram using simple analytical arguments. For further progress, it would be important to determine the flow field near the tip of the foil and in the boundary layers on the sides and to further develop the description of the vorticity formation in the boundary layers and at the trailing edge. This would provide important input for the development of models with few degrees of freedom and for a theoretical understanding of the drag–thrust transition. Also it would be interesting to determine to what extent the observed 2P wakes are associated with drag or thrust and to see if the timing of the vortex formation at the round leading edge and the trailing edge can be tuned so that thrust can be produced in a region like the small 2P island below the well-known drag–thrust transition line in the phase diagram. Due to the inherent complexity of soap film flows it would be important, for these more detailed studies, to complement the soap film experiments with numerical simulations and experiments in water tunnels using, e.g., particle image velocimetry and force measurements. Here our results could serve as an effective guide to the pertinent structures and transitions. The soap film also provides a detailed view of the far-wake evolution, and it would be interesting to compare with analytical solutions of point vortex models to describe, e.g., the 2P wake evolution in which vortex pairs move away from the centreline and slowly turn downstream.

We thank Hassan Aref, Laust Tophøj and Jun Zhang for many fruitful discussions, and we are indebted to Erik Hansen for his careful construction of the experimental set-up.

REFERENCES

Anderson, J. M., Streitlien, K., Barrett, D. S. & Triantafyllou, M. S. 1998 Oscillating foils of high propulsive efficiency. *J. Fluid Mech.* **360**, 41–72.

Aref, H., Stremler, M. A. & Ponta, F. L. 2006 Exotic vortex wakes – point vortex solutions. *J. Fluids Struct.* **22**, 929–940.

Bohl, D. G. & Koochesfahani, M. M. 2009 MTV measurements of the vortical field in the wake of an airfoil oscillating at high reduced frequency. *J. Fluid Mech.* **620**, 63–88.

Bratt, J. B. 1953 Flow patterns in the wake of an oscillating aerofoil. *Aero. Res. Counc. R. M.* **2773**, 1–28.

Buchholz, J. H. J. & Smits, A. J. 2008 The wake structure and thrust performance of a rigid low-aspect-ratio pitching panel. *J. Fluid Mech.* **603**, 331–365.

Chomaz, J.-M. & Cathalau, B. 1990 Soap films as two-dimensional classical fluids. *Phys. Rev.* A **41**, 2243–2245.

Couder, Y. & Basdevant, C. 1986 Experimental and numerical study of vortex couples in two-dimensional flows. *J. Fluid Mech.* **173**, 225–251.

Couder, Y., Chomaz, J.-M. & Rabaud, M. 1989 On the hydrodynamics of soap films. *Physica* D **37**, 384–405.

Garrick, I. E. 1936 Propulsion of a flapping and oscillating airfoil. *Rep. No.* **567**. NACA.

Gharib, M. & Derango, P. 1989 A liquid film (soap film) tunnel to study two-dimensional laminar and turbulent shear flows. *Physica* D **37**, 406–416.

Godoy-Diana, R., Aider, J.-L. & Wesfreid, J. E. 2008 Transitions in the wake of a flapping foil. *Phys. Rev.* E **77**, 016308.

Godoy-Diana, R., Marais, C., Aider, J.-L. & Wesfreid, J. E. 2009 A model for the symmetry breaking of the reverse Benard–von Kármán vortex street produced by a flapping foil. *J. Fluid Mech.* **622**, 23–32.

von Kármán, T. & Burgers, J. M. 1935 General aerodynamic theory – perfect fluids. In *Aerodynamic Theory II*, pp. 280–310 (ed. by W. F. Durand). Dover Publications, 1963.

Koochesfahani, M. M. 1986 Wake of an oscillating airfoil. *Phys. Fluids* **29**, 2776.

Koochesfahani, M. M. 1989 Vortical patterns in the wake of an oscillating airfoil. *AIAA J.* **27**, 1200–1205.

Lai, J. C. S. & Platzer, M. F. 1999 Jet characteristics of a plunging airfoil. *AIAA J.* **37**, 1529–1537.

Lentink, D., Muijres, F. T., Donker-Duyvis, F. J. & van Leeuwen, J. L. 2008 Vortex–wake interactions of a flapping foil that models animal swimming and flight. *J. Exp. Biol.* **211**, 267–273.

Lighthill, M. J. 1969 Hydromechanics of aquatic animal propulsion. *Annu. Rev. Fluid Mech.* **1**, 413–446.

Müller, U. K., van den Boogaart, J. G. M. & van Leeuwen, J. L. 2008 Flow patterns of larval fish: undulatory swimming in the intermediate flow regime. *J. Exp. Biol.* **211**, 196–205.

Müller, U. K., Smit, J., Stamhuis, E. J. & Videler, J. J. 2001 How the body contributes to the wake in undulatory fish swimming: flow fields of a swimming eel (*Anguilla anguilla*). *J. Exp. Biol.* **204**, 2751–2762.

Ponta, F. L. & Aref, H. 2005 Vortex synchronization regions in shedding from an oscillating cylinder. *Phys. Fluids* **17**, 011703.

Prandtl, L. & Tietjens, O. G. 1934 *Fundamentals of Hydro- and Aeromechanics*. Dover Publications.

Rivera, M., Vorobieff, P. & Ecke, R. E. 1998 Turbulence in flowing soap films: velocity, vorticity, and thickness fields. *Phys. Rev. Lett.* **81**, 1417–1420.

Rutgers, M. A., Wu, X. L. & Daniel, W. B. 2001 Conducting fluid dynamics experiments with vertically falling soap films. *Rev. Sci. Instrum.* **72**, 3025–3037.

Sfakiotakis, M., Lane, D. M. & Davies, J. B. C. 1999 Review of fish swimming modes for aquatic locomotion. *IEEE J. Oceanic Engng* **24**, 237–252.

Triantafyllou, M. S., Triantafyllou, G. S. & Yue, D. K. P. 2000 Hydrodynamics of fishlike swimming. *Annu. Rev. Fluid Mech.* **32**, 33–53.

Vorobieff, P. & Ecke, R. E. 1999 Cylinder wakes in flowing soap films. *Phys. Rev.* E **60**, 2953–2956.

Williamson, C. H. K. & Roshko, A. 1988 Vortex formation in the wake of an oscillating cylinder. *J. Fluids Struct.* **2**, 355–381.

Zhang, J., Childress, S., Libchaber, A. & Shelley, M. 2000 Flexible filaments in a flowing soap film as a model for one-dimensional flags in a two-dimensional wind. *Nature* **408**, 835–839.